NAOJ-Th-Ap2001, No.18
Preprint typeset using LaTeX style emulateapj v. 14/09/00

GALAXY NUMBER COUNTS IN THE HUBBLE DEEP FIELD AS A STRONG CONSTRAINT ON A HIERARCHICAL GALAXY FORMATION MODEL

MASAHIRO NAGASHIMA,[1] TOMONORI TOTANI AND NAOTERU GOUDA
National Astronomical Observatory, Mitaka, Tokyo 181-8588, Japan; masa@th.nao.ac.jp

AND

YUZURU YOSHII
Institute of Astronomy, School of Science, The University of Tokyo, 2-21-1 Osawa, Mitaka, Tokyo 181-8588, Japan
Research Center for the Early Universe, Faculty of Science, The University of Tokyo, Tokyo 113-0033, Japan
NAOJ-Th-Ap2001, No.18

ABSTRACT

Number counts of galaxies are re-analyzed using a semi-analytic model (SAM) of galaxy formation based on the hierarchical clustering scenario. We have determined the astrophysical parameters in the SAM that reproduce observations of nearby galaxies, and used them to predict the number counts and redshifts of faint galaxies for three cosmological models for (1) the standard cold dark matter (CDM) universe, (2) a low-density flat universe with nonzero cosmological constant, and (3) a low-density open universe with zero cosmological constant. The novelty of our SAM analysis is the inclusion of selection effects arising from the cosmological dimming of surface brightness of high-redshift galaxies, and also from the absorption of visible light by internal dust and intergalactic H I clouds. Contrary to previous SAM analyses which do not take into account such selection effects, we find, from comparison with observed counts and redshifts of faint galaxies in the Hubble Deep Field (HDF), that the standard CDM universe is *not* preferred, and a low-density universe either with or without cosmological constant is favorable, as suggested by other recent studies. Moreover, we find that a simple prescription for the time scale of star formation (SF), being proportional to the dynamical time scale of the formation of the galactic disk, is unable to reproduce the observed number- redshift relation for HDF galaxies, and that the SF time scale should be nearly independent of redshift, as suggested by other SAM analyses for the formation of quasars and the evolution of damped Ly-α systems.

Subject headings: cosmology: theory – galaxies: evolution – galaxies: formation – large-scale structure of universe

1. INTRODUCTION

In the field of observational cosmology, counts of the number of faint galaxies in a given area of sky provide one of the most fundamental observables from which the cosmological parameters, and hence the geometry of the Universe, can be determined (e.g., Peebles 1993). The predicted number counts of galaxies as a function of apparent magnitude and redshift, which should be compared with the data, is obtained from summing up the derived luminosity functions over all redshifts and morphological types, then multiplied by a redshift-dependent cosmological volume element. While the local luminosity function of galaxies of individual types is known from redshift surveys, the luminosity function at any high redshift still has to be deduced with the help of morphological-type-dependent evolution models of galaxies. Accordingly, the predicted number counts rely directly on how well the evolution of galaxies is modeled from their formation until the present (e.g., Yoshii & Takahara 1988).

With the usual assumption of monolithic collapse, the wind model for elliptical galaxies and the infall model for spiral galaxies are able to reproduce many of the observed properties of nearby galaxies, and provide a strong theoretical tool for understanding their evolution (Arimoto & Yoshii 1986, 1987; Arimoto, Yoshii,& Takahara 1991). However, when using these traditional evolution models, it has been claimed that the standard cold dark matter (CDM) universe, or the Einstein-de Sitter (EdS) universe, is not reconciled with the observed high counts of faint galaxies, and that a low-density universe is preferred (Yoshii & Takahara 1988; Yoshii & Peterson 1991, 1995; Yoshii 1993). Most recently, Totani & Yoshii (2000, hereafter TY00) compared their predictions against the number counts observed to the faint limits in the Hubble Deep Field (HDF, Williams et al. 1996) by taking into account various selection effects for the first time. Allowing for the possibility of number evolution of galaxies in a phenomenological way, and after a comprehensive check of systematic model uncertainties, they strengthened previous claims and further demonstrated that mild or negligible merging of high-redshift galaxies in a low-density flat universe with nonzero cosmological constant is a likely solution to simultaneously reproduce the observed high counts and redshift distribution of faint galaxies. On the other hand, the EdS universe is in serious contradiction with the data even if a strong number evolution is invoked.

However, there is a growing evidence from recent observations of the large-scale structure of the universe that gravitationally bound objects, such as galaxy clusters, are formed through continuous mergers of dark halos. Some authors have tried to construct a galaxy formation model based on this scenario of hierarchical clustering in a CDM universe, referred to as a semi-analytic model (SAM) of galaxy formation (e.g., Kauffmann, White, & Guiderdoni 1993; Cole et al. 1994). In fact, SAMs successfully reproduced a variety of observed features of local galaxies such as their luminosity function, color distribution, and so on.

The number counts of faint galaxies have also been analyzed using SAMs (Cole et al. 1994; Kauffmann, Guiderdoni & White 1994; Heyl et al. 1995; Baugh, Cole & Frenk 1996).

The Durham group claimed that their model agrees with the observed number counts in the EdS universe rather than in a low-density universe. The Munich group reached a similar conclusion by halting the process of star formation in smaller halos with circular velocities less than 100 km s^{-1}. These conclusions by both groups are apparently at variance with those obtained using the traditional evolution models of galaxies. This apparent discrepancy needs to be immediately resolved.

In this paper we examine the importance of selection effects in observations of faint galaxies which have been ignored in previous SAM analyses of galaxy number counts, such as the cosmological dimming of surface brightness and the absorption of emitted light by internal dust and intergalactic H I clouds. Taking into account these effects in the same way as in TY00, our SAM analysis obtains, for the first time, the predicted number counts that can be consistently compared with the HDF counts to faint magnitude limits.

This paper is outlined as follows. In §2 we briefly describe our SAM. In §3 we constrain the astrophysical parameters in our SAM analysis against local observations. In §4 we compare theoretical number counts and redshift distributions of faint galaxies with the data, and discuss the range of uncertainties in our calculations of galaxy counts. In §5 we provide a summary and discussion.

2. MODEL

The SAM we employ involves known physical processes connected with the process of galaxy formation. It is therefore straightforward to understand how galaxies form and evolve within the context of this model. In the CDM universe, dark matter halos cluster gravitationally and are merged in a manner that depends on the adopted power spectrum of initial density fluctuations. In each of the merged dark halos, radiative gas cooling, star formation, and gas reheating by supernovae occur. The cooled dense gas and stars constitute *galaxies*. These galaxies sometimes merge together in a common dark halo and more massive galaxies form.

For the purpose of comparison with observation, we use a stellar population synthesis approach, from which the luminosities and colors of model galaxies are calculated. The SAM well explains the local luminosity function of galaxies, the color distribution, and so on. Our present SAM analysis obtains essentially the same results of previous SAM analyses, with minor differences in a number of details. In this section we only briefly describe our model; its full description will be given in Nagashima & Gouda (2001, in preparation).

2.1. *Scheme of Galaxy Formation*

First, based on the method of Somerville & Kolatt (1999), we determine the merging history of dark matter halos by extending the Press-Schechter formalism (Press & Schechter 1974; Bower 1991; Bond et al. 1991; Lacey & Cole 1993). We adopt the power spectrum for a specific cosmology from Bardeen et al. (1986), and assume a halo with circular velocity $V_{\rm circ} < 40$km s^{-1} as a diffuse accretion entity. The evolution of the baryonic component is followed until the output redshift with the redshift interval of $\Delta z = 0.06(1+z)$, corresponding to the dynamical time scale of halos which collapse at that time. In order to minimize the artificial effect of dividing the history of galaxy formation into discrete redshift intervals, we fix $\Delta z = 0.06$ until just prior to the output redshift. This manipulation is important especially at high redshift. In our analysis, the highest output redshift is $z \simeq 9$ with the interval of the output redshift $\sim$0.05-0.4.

If a dark matter halo has no progenitor halos, the mass fraction of the gas is given by $\Omega_{\rm b}/\Omega_0$, where Ω_0 is the density parameter for the total baryonic and non-baryonic components, and $\Omega_{\rm b} = 0.015h^{-2}$ is the baryonic density parameter constrained by primordial nucleosynthesis calculations (e.g., Suzuki, Yoshii, & Beers 2000). In this work h represents the Hubble parameter given by $h = H_0/100$ km s^{-1}Mpc^{-1}.

When a dark matter halo collapses, the gas in the halo is shock-heated to the virial temperature of the halo. We refer to this heated gas as the *hot gas*. At the same time, the gas in dense regions of the halo is cooled due to efficient radiative cooling. We call this cooled gas the *cold gas*. Assuming an isothermal density distribution of the entire halo and using the metallicity-dependent cooling function by Sutherland & Dopita (1991), we calculate the amount of cold gas which eventually falls onto a central galaxy in the halo. In order to avoid the formation of unphysically large galaxies, the above cooling process is applied only to halos with $V_{\rm circ} < 500$ km s^{-1} in the standard CDM and 400 km s^{-1} in low-density universes. The physical reason for this restriction is not clear, but Cole et al. (2000a) recently reported that the formation of enormous galaxies is hindered in the isothermal halo having a large core. Nevertheless, in this paper we adopt a simple isothermal distribution and prevent the formation of so-called "monster galaxies" by hand.

Stars are formed from the cold gas at a rate of $\dot{M}_* = M_{\rm cold}/\tau_*$, where $M_{\rm cold}$ is the mass of cold gas and τ_* is the time scale of star formation. We assume that τ_* is independent of z, but dependent on $V_{\rm circ}$ as follows:

$$\tau_* = \tau_*^0 \left(\frac{V_{\rm circ}}{300{\rm km\ s^{-1}}} \right)^{\alpha_*}. \qquad (1)$$

This form is referred to as the "Durham model" by Somerville & Primack (1999). It should be noted that Cole et al. (2000a) modified their original form (equation 1) as

$$\tau_* = \tau_*^0 \left(\frac{V_{\rm circ}}{200{\rm km\ s^{-1}}} \right)^{\alpha_*} \left(\frac{\tau_{\rm dyn}(z)}{\tau_{\rm dyn}(0)} \right), \qquad (2)$$

by multiplying a factor proportional to the dynamical time scale in the galactic disk. This form is similar to "Munich model" (Kauffman, White & Guiderdoni 1993).

For convenience, the cases in equations (1) and (2) are hereafter referred to as "constant star formation (CSF)" and "dynamical star formation (DSF)," respectively. The free parameters of τ_*^0 and α_* in CSF and DSF are fixed by matching the observed mass fraction of cold gas in neutral form in the disks of spiral galaxies. Cole et al. (2000a) stressed that the $V_{\rm circ}$-dependence is needed to reproduce the observed ratio of gas mass relative to the B-band luminosity of a galaxy. The effect of introducing the $\tau_{\rm dyn}$-dependence in DSF will be discussed in §4.2.1.

In our SAM, stars with masses larger than $10M_\odot$ explode as Type II supernovae (SNe) and heat up the surrounding cold gas. This SN feedback reheats the cold gas to hot gas at rate of $\dot{M}_{\rm reheat} = M_{\rm cold}/\tau_{\rm reheat}$, where the time scale of reheating is given by

$$\tau_{\rm reheat} = \left(\frac{V_{\rm circ}}{V_{\rm hot}} \right)^{\alpha_{\rm hot}} \tau_*. \qquad (3)$$

The free parameters of $V_{\rm hot}$ and $\alpha_{\rm hot}$ are determined by matching the local luminosity function of galaxies.

With these $\dot{M}_*$ and $\dot{M}_{\rm reheat}$ thus determined, we obtain the masses of hot gas, cold gas, and disk stars as a function of time during the evolution of galaxies. Chemical enrichment is also taken into account adopting *heavy-element yield* of $y = 0.038 = 2Z_\odot$, but changing this value of y has a minimal effect on the results described below.

When two or more progenitor halos have merged, the newly formed larger halo should contain at least two or more galaxies which had originally resided in the individual progenitor halos. By definition, we identify the central galaxy in the new common halo with the central galaxy contained in the most massive of the progenitor halos. Other galaxies are regarded as satellite galaxies.

These satellites merge by either dynamical friction or random collision. The time scale of merging by dynamical friction is given by

$$\tau_{\rm fric} = \frac{260}{\ln\Lambda_{\rm c}} \left(\frac{R}{\rm Mpc}\right)^2 \left(\frac{V_{\rm circ}}{10^3 {\rm km\ s^{-1}}}\right) \left(\frac{M_{\rm sat}}{10^{12} M_\odot}\right)^{-1} {\rm Gyr}, \quad (4)$$

where R and $V_{\rm circ}$ are the radius and the circular velocity of the new common halo, respectively, $\ln\Lambda_{\rm c}$ is the Coulomb logarithm, and $M_{\rm sat}$ is the mass of the satellite galaxies including the mass of dark matter (Binney & Tremain 1987). When the time elapsed after a galaxy becomes a satellite exceeds $\tau_{\rm fric}$, a satellite galaxy infalls onto the central galaxy. On the other hand, the mean free time scale of random collision is given by

$$\tau_{\rm coll} = \frac{500}{N^2} \left(\frac{R}{\rm Mpc}\right)^3 \left(\frac{r_{\rm gal}}{0.12{\rm Mpc}}\right)^{-2} \times \left(\frac{\sigma_{\rm gal}}{100{\rm km\ s^{-1}}}\right)^{-4} \left(\frac{\sigma_{\rm halo}}{300{\rm km\ s^{-1}}}\right)^3 {\rm Gyr}, \quad (5)$$

where N is the number of satellite galaxies, $r_{\rm gal}$ is their radius, and $\sigma_{\rm halo}$ and $\sigma_{\rm gal}$ are the 1D velocity dispersions of the common halo and satellite galaxies, respectively (Makino & Hut 1997). For simplicity, the satellite radius $r_{\rm gal}$ is set to be one tenth of the virial radius of a progenitor halo to which the satellite once belonged as a central galaxy. With a probability $\Delta t/\tau_{\rm coll}$, where Δt is the time step corresponding to the redshift interval Δz, a satellite galaxy merges another satellite picked out randomly. This process was first introduced in a SAM by Somerville & Primack (1999).

Consider the case that two galaxies of masses m_1 and $m_2 (> m_1)$ merge together. If the mass ratio $f = m_1/m_2$ is larger than a certain critical value of $f_{\rm bulge}$, we assume that a starburst occurs and all the cold gas turns into hot gas, which fills in the halo, and the stars populate the bulge of a new galaxy. On the other hand, if $f < f_{\rm bulge}$, no starburst occurs and a smaller galaxy is simply absorbed into the disk of a larger galaxy. These processes are repeated until the output redshift.

Given the SF rate as a function of time or redshift, the absolute luminosity and colors of individual galaxies are calculated using a population synthesis code by Kodama & Arimoto (1997). The stellar metallicity grids in the code cover a range of Z_* =0.0001-0.05. The initial stellar mass function (IMF) that we adopt is the power-law IMF of Salpeter form with lower and upper mass limits of $0.1{\rm M}_\odot$ and $60{\rm M}_\odot$, respectively. Since our knowledge of the lower mass limit is incomplete, there is the possibility that many brown dwarf-like objects are formed. Therefore, following Cole et al. (1994), we introduce a parameter defined as $\Upsilon = (M_{\rm lum} + M_{\rm BD})/M_{\rm lum}$, where $M_{\rm lum}$ is the total mass of luminous stars with $m \geq 0.1 M_\odot$ and $M_{\rm BD}$ is that of invisible brown dwarfs.

To account for extinction by internal dust we adopt a simple model by Wang & Heckman (1996) in which the optical depth in B-band is related to the luminosity as $\tau_B = 0.8(L_B/1.3 \times 10^{10} L_\odot)^{0.5}$. Optical depths in other bands are calculated by using the Galactic extinction curve, and the dust distribution in disks is assumed to be the slab model considered by Somerville & Primack (1999). It is not trivial that such an empirical dust model can be extraporated to very bright galaxies. However, since the extinction is typically $A_B \sim 1$ mag at the bright-end of the local luminosity function, our results especially in the I-band are not significantly affected by the details of the dust model.

Emitted light from distant galaxies is absorbed by Lyman lines and Lyman continuum in intervening intergalactic H I clouds. The redshift at which this effect becomes important is different for different photometric passbands, because the absorption occurs around 1000 A in the rest frame of the clouds. Fig. A1 shows the expected extinction as a function of redshift for four passband filters of the HDF (Yoshii & Peterson 1994). This effect has been included into a SAM by Baugh et al. (1998) in order to pick out the Lyman-break galaxies at high redshift by color selection criteria.

We classify galaxies into different morphological types according to the B-band bulge-to-disk luminosity ratio B/D. In this paper, following Simien & de Vaucouleurs (1986), galaxies with $B/D \geq 1.52$, $0.68 \leq B/D < 1.52$, and $B/D < 0.68$ are classified as ellipticals, S0s, and spirals, respectively. Kauffmann et al. (1993) and Baugh, Cole & Frenk (1996) showed that this method of type classification well reproduces the observed type mix.

The above procedure is a standard one in the SAM of galaxy formation. In the next subsection, in order to investigate the properties of high-z galaxies properly, we introduce two important effects into our SAM analysis.

2.2. *New ingredients of the model: selection effects*

We judge whether the surface brightness of the galaxies in our SAM is above the detection threshold of the HDF observations. The intrinsic size of spiral or disk-dominated galaxies is estimated by adopting the dimensionless spin parameter $\lambda_{\rm H} = 0.05$, and by conserving the specific angular momentum during the gas cooling. On the other hand, the intrinsic size of early-type galaxies is estimated from their virial radii, adjusted by a scaling parameter $f_{\rm b}$ to match with the observed size of early-type galaxies. Note that the selection effects on the local luminosity function have been considered by Cole et al. (2000a) in a simple way in which the isophotal magnitude within 25 mag arcsec^{-2} was used.

The selection effects in predicting the HST number counts in our SAM analysis are evaluated as follows. Using the intrinsic size of model galaxies as obtained above, and adopting a Gaussian point-spread function $f(x)$ for the HST observations, the surface brightness profile $\tilde{g}(x)$ in the observer frame is given by

$$\tilde{g}(|\mathbf{x}|) = \int {\rm d}\mathbf{x}' f(|\mathbf{x}' - \mathbf{x}|) g(|\mathbf{x}'|), \quad (6)$$

where $|\mathbf{x}| = x = r/r_{\rm e}$ is the normalized radius away from the galaxy center relative to the effective radius $r_{\rm e}$, and $g(x) = \exp(-a_n x^{1/n})$ is the intrinsic surface brightness profile. We adopt $n = 1$ for spirals and $n = 4$ for ellipticals. The coefficient a_n is given by $a_1 = 1.68$ and $a_4 = 7.67$. Then, for each of our model galaxies, we determine their surface brightness

profile $S(\theta)$, where $\theta = xr_e/d_A$ and d_A is the angular-diameter distance. We note that model galaxies with surface brightness brighter than the threshold S_{th} and with an isophotal diameter larger than the minimum diameter D_{min} are actually detected as galaxies (Yoshii 1993). In order to be consistent with the HDF observations, we use the isophotal magnitude scheme, S_{th} = 27.5 mag arcsec^{-2} in V_{606}, S_{th} = 27.0 mag arcsec^{-2} in I_{814}, U_{300} and B_{450}, and $D_{min} \sim$0.2 arcsec. More details are described in TY00.

3. THE SETTING OF PARAMETERS IN OUR SAM ANALYSIS

We consider the predicted number counts in four models – SC, OC, LC, and LD (Table A1). The first three models are for CSF (equation 1), and the fourth model is for DSF (equation 2). The capitals S, O, and L refer to the standard CDM universe, a low-density open universe and a low-density flat universe with non-zero cosmological constant (Λ), respectively.

The cosmological parameters (Ω_0, Ω_Λ, h, σ_8) are tabulated in Table A1. For all the models the baryon density parameter $\Omega_b = 0.015h^{-2}$ is used in common. For the low-density open and flat universes the value of σ_8 is determined from observed cluster abundances (Eke, Cole & Frenk 1996).

The astrophysical parameters (V_{hot}, α_{hot}, τ_*^0, α_*, f_b, f_{bulge}, Υ) are constrained from local observations. However, since the parameter of f_{bulge}, among others, do not affect our result, we set f_{bulge} = 0.2 for the standard CDM universe, and f_{bulge} = 0.5 for the low-density open and flat universes. Other parameters are discussed below.

3.1. *The Local Luminosity Function of Galaxies*

The SN feedback-related parameters of V_{hot} and α_{hot} determine the location of the knee of the luminosity function and the faint-end slope, respectively. It should be noted that the mass fraction Υ of invisible stars determines the magnitude scale of galaxies, so that changing Υ moves the luminosity function horizontally without changing its overall shape. Therefore, coupled with V_{hot}, Υ determines the bright portion of the luminosity function.

Fig. A2 shows theoretical results represented by thick lines for the four models tabulated in Table A1. Symbols with errorbars indicate observational results from the *B*-band redshift surveys such as APM (Loveday et al. 1992), ESP (Zucca et al. 1997), Durham/UKST (Ratcliffe et al. 1997), 2dF (Folkes et al. 1999) and SDSS (Blanton et al. 2000), and from the *K*-band redshift surveys (Mobasher et al. 1993; Gardner et al. 1997; 2MASS, Cole et al. 2000b). It is evident that while most of *B*-band redshift surveys give a rather flat slope in the faint end, the ESP and SDSS surveys give an extreme case showing a much steeper slope. Note that the SDSS luminosity function shown in Fig. A2 is that with the same detection limit as employed in the 2dF survey.

In this paper we have chosen the values of SN feedback-related parameters so as to reproduce a flat faint-end slope, but in §4.2.3 we will investigate the effect of using the steepest ESP slope in predicting the number counts of faint galaxies.

3.2. *The Mass Fraction of Cold Gas in Spiral Galaxies*

The SF rate-related parameters of τ_*^0 and α_* determine the overall mass fraction of cold gas in galaxies with given luminosity and its luminosity dependence, respectively. In some previous SAM analyses, the mass fraction of gas in the Milky Way is exclusively used to fix τ_*^0 for all other spiral galaxies. Then, when $\alpha_* = 0$, Cole et al. (2000a) found that dwarf-size galaxies have too little gas to be consistent with observations. According to Cole et al. (2000a), we here constrain both τ_*^0 and α_* in a combined manner to reproduce the mass fraction of cold gas in galaxies spanning a wide range of luminosity.

Fig. A3 shows the ratio of cold gas mass relative to *B*-band luminosity of spiral galaxies as a function of their luminosity. Solid curves show theoretical results for the four models tabulated in Table A1. We here assume that 75% of the cold gas in these models is comprised of hydrogen, i.e., $M_{HI} = 0.75M_{cold}$. Filled diamonds with errorbars indicate the H I data taken from Huchtmeier & Richter (1988).

It should be noted that use of τ_*^0 for either CSF (equation 1) or DSF (equation 2) hardly affects the resulting luminosity function, as seen from the difference between LC and LD in Fig. A2. However, α_* depends on the strength of the SN feedback, and the strength should be different for different universe models (see Table A1). Therefore, in the case of α_*, we can only fix its value after the SN feedback-related parameters are constrained in a specified universe model.

3.3. *The Intrinsic Sizes of Galaxies*

The scaling parameter f_b is determined by matching the effective radius of early-type L_* galaxies, while the actual L-dependence in f_b is ignored for simplicity. We discuss the effect of this assumption in §4.2.2.

Knowledge of the intrinsic size of galaxies is a necessary quantity in our SAM analysis, because it is the surface brightness of galaxies, not their luminosity, that is relevant to evaluating the selection effects for model galaxies. For spiral galaxies, the key process is the conservation of specific angular momentum during the cooling of hot gas. The effective disk radius r_e is given by $r_e = (1.68/\sqrt{2})\lambda_H r_i$, where r_i is an initial radius of the progenitor gas sphere (Fall 1983). However, the definition of disk size during the cooling phase is not readily apparent from this formula. Furthermore, the angular momentum transfer during mergers of galaxies in a merged halo is very complicated. Without entering into all these complexities, in this paper we re-estimate the disk size by the above equation when the disk mass increases twice. This approach is simple but reproduces the observations rather well.

Fig. A4 shows the effective disk radii of spiral galaxies as a function of their luminosity. Thick solid lines show the theoretical results for the four models tabulated in Table A1. Dotted lines indicate the best-fit relation to the observational data given by Impey et al. (1996). All models provide reasonable disk sizes for dwarf galaxies. Slight deviations from the observations of bright galaxies may have occurred partly because dust obscuration becomes effective for such galaxies (cf. §2.2), and partly because our method of defining the disk size is too simple. We discuss the effect of changing the disk size in §4.2.2.

In this paper, the effective radius of elliptical galaxies is estimated from scaling the virial radius by a parameter f_b, i.e., $r_e = f_b GM_b/V_{circ}^2$, where M_b is the mass of stars and cold gas, and f_b is fixed to reproduce the effective radius of an L_* galaxy. In Fig. A4, thick dashed lines indicate the effective radius of elliptical galaxies for the four models tabulated in Table A1. Dashed and dot-dashed lines show the best-fit relations for dwarf and compact ellipticals, respectively, based on the observational data given by Bender et al. (1992). Unfortunately, our SAM analysis cannot reproduce two distinct sequences simultaneously; the theoretical $r_e - L_B$ relation becomes coincident

with the bright portion of the giant-dwarf sequence, whereas the same relation changes its slope becoming coincident with the faint portion of giant-compact sequence. We find that this changeover magnitude is determined by the strength of SN feedback (see Appendix A), and that the extreme manipulation that reproduce the dwarf sequence affects the number counts of model galaxies only weakly.

4. RESULTS

4.1. *Galaxy Number Counts*

Fig. A5 shows the number counts of galaxies as a function of apparent isophotal magnitude for the SC, OC, and LC models in the HST *UBVI* bands in the AB magnitude system. The thick lines are the theoretical predictions, based on the HST observational conditions, including the selection effects from the cosmological dimming of surface brightness and also from the absorption of visible light by internal dust and intergalactic H I clouds. The thin lines are the predictions ignoring the selection effects except for the effect of dust absorption, because the dust absorption is already taken into account in reproducing the local luminosity function. Open circles with errorbars show the HDF data (Williams et al. 1996), and other symbols show ground-based data after transformation to AB magnitudes to be consistent with the HST.

In order to discriminate favorable universe models, the predictions shown by the thick lines should be compared directly with the observational data. It is evident from this figure that the SC model falls short of the HST data. We note that the discrepancy between the SC model and the data is seen at $B_{450} \gtrsim 25$, even if we do not consider the selection effects. On the other hand, both of the LC and OC models agree well with the data, owing to the inclusion of selection effects. We will discuss the uncertainty of estimating these effects in the next section.

Fig. A6 shows the redshift distribution of galaxies. The thick lines denote the SC, OC and LC models, including all the selection effects as in Fig. A5. The histogram indicates the observed redshift distribution based on photometric redshifts of HDF galaxies estimated by Furusawa et al. (2000), in which they improved the method of redshift estimation compared to the method by Fernández-Soto, Lanzetta & Yahil (1999).

In the LC model, both the peak height and the distribution towards higher redshift agree well with the observation. However, the peak height of the SC model falls significantly short of that observed at $z \simeq 1-1.5$. This is a direct reflection of the lack of galaxies in the theoretical number-magnitude relation for the SC model (see Fig.A5). In the OC model, the relative number between the peak and high-z tail at $z \gtrsim 3$ is smaller than that observed and is inconsistent with the data. This is a direct reflection of the z-dependence of the comoving volume element dV/dz, which is shown in the middle panel of Fig.A6. While in the LC model the matter density dominates over the cosmological constant at high redshift, which leads to a similar z-dependence of dV/dz to that in the EdS universe, the negative curvature effect makes dV/dz decline more slowly at such high redshift in the OC model. Thus the redshift distribution in the OC model declines toward higher redshift more slowly than that in the LC model. In order for the OC model to agree with the data, we would need to halt the star formation at $z \gtrsim 3$ by hand, for unknown reasons.

We conclude that as far as that the astrophysical parameters in our SAM analysis are constrained by local luminosity function of galaxies, the standard CDM universe does not agree with both the observed number-magnitude and number-redshift relations, and that the Λ-dominated flat universe is best able to reproduce these relations simultaneously.

4.2. *Uncertainties in the SAM counts*

In this section we discuss uncertainties in predicting the number counts of galaxies. Sources of such uncertainties considered here include the time scale of star formation (§4.2.1), the galaxy size (§4.2.2), and the adopted SN feedback (§4.2.3).

4.2.1. *Star Formation Time-Scale*

Here we evaluate the effects of changing the time-scale of star formation from CSF (equation 1) to DSF (equation 2). Fig. A7 shows predicted number counts for the corresponding Λ-dominated LC and LD models. The difference between these models is apparently small but its magnitude-dependence is different among the predictions in the *UBVI* bands. In the case of longer wavelength such as the I_{814} band, the number of faint galaxies in the LD model becomes larger than that in the LC model, because in the case of DSF more stars are formed at high redshift according to much a shorter $\tau_*(\mathrm{DSF})$ as compared with CSF. [In the particular case of the EdS universe, not shown here, the DSF gives $\tau_*(\mathrm{DSF}) \propto (1+z)^{-3/2}$, so that the present $\tau_*(\mathrm{DSF})$ is more than 10 times longer than that at $z \sim 5$.] However, in the case of shorter wavelengths, particularly the U_{300} band, because the apparent luminosity from galaxies is dominated by instantaneous SF, and because many stars have already been formed at higher redshift, the number of faint galaxies in the LD model becomes slightly smaller than that in the LC model.

The difference between the LC and LD models is most prominent when we consider the redshift distribution of faint galaxies. Fig. A8 shows such predictions for the LC and LD models. Clearly the LD model predicts too many high-z galaxies to be consistent with observation. We may be able to remedy this defect by imposing a more efficient internal dust absorption in order to decrease the number of high-z galaxies. However, this manipulation simply decreases the number of faint galaxies below that observed in the U_{300}. Thus, we suggest that the z-dependence of SF should be negligible and the CSF is a reasonable option in the framework of our SAM.

4.2.2. *Galaxy Size*

In this paper, it is assumed according to the usual SAM analysis that the physical mechanism for determining the galaxy size is the conservation of specific angular momentum for spiral galaxies and the virial theorem for the baryon component of elliptical galaxies. While this assumption is considered to be reasonable, it is important to note the uncertainties in the normalization of the above relations. In this section we consider two LC variants and compare them with the original LC model. Figs. A9 and A10 present theoretical predictions from these three LC models. We rather arbitrarily decrease and increase the original galaxy size by a factor of 2, and refer to these variants as "high surface brightness" and "low surface brightness," respectively. Note that the 1σ scatter in the observational data is about a factor of 1.7, so the range of changing the radius is sufficient large to check the uncertainty in the galaxy size. Given the threshold of surface brightness for detection used in the HST observation, model galaxies with "high surface brightness" are more easily detected, while those with "low surface brightness" remain undetected. The number counts of these two

variants differ only by a factor of 1.5 at $B_{450} \sim 28$, as well as at the corresponding magnitudes in the other bands. We found that the uncertainties from changing the galaxy size in the SC and OC models are almost the same as those in the LC model.

4.2.3. *Supernova Feedback*

The SN feedback-related parameters essentially determine the resulting shape of the local luminosity function of galaxies (§3.1). Therefore, changing these parameters corresponds to changing the number density of galaxies in the local universe. In this section, we constrain these parameters against the ESP luminosity function (Zucca et al. 1997) which gives the steepest faint-end slope among other observations. This is done by weakening the strength of SN feedback in three CSF variants such as SCw, OCw, and LCw. Other parameters such as the SF rate-related are determined by the same way in §3. All the parameters for these models are tabulated in Table A2, and their *B*-band luminosity functions are shown in Fig. A11.

Straightforward calculations predict the number counts of galaxies which exceed the bright counts at $B \sim 20$, and this excess alone may invalidate the extreme assumption for faint-end slope of the local luminosity function. However, considering the possible existence of systematic uncertainties that could affect current observations of the local luminosity function, we adjust the normalization in such a way as to reproduce the observed bright counts. Then we examine the effect of adopting the steepest ESP slope instead of our standard choice. Fig. A12 shows the number counts of galaxies for the SCw, OCw, and LCw models. It is evident from this figure that even the steepest ESP slope does not save the standard CDM universe, which confirms the claim by TY00.

5. SUMMARY AND DISCUSSION

We have calculated the number counts of faint galaxies in the framework of a SAM for three cosmological models of the standard CDM (EdS) universe, a low-density open universe, and a low-density flat universe with nonzero Λ. The novelty of our SAM analysis is that theoretical predictions are made by fully taking into account the selection effects from the cosmological dimming of surface brightness of galaxies and also from the absorption of visible light by internal dust and intergalactic H I clouds.

Comparison of theoretical predictions with the observed number counts and photometric redshift distribution of HST galaxies, as well as other ground-based observations, indicates that the standard CDM is ruled out and a Λ-dominated flat universe is most favorable, while a low-density open universe is marginally favored. This result is in sharp contrast with previous SAM analyses on galaxy number counts where many of the conceivable selection effects in faint observations have been ignored. It is only recently that the SAM analyses have included the effects of internal dust absorption (Somerville & Primack 1999; Cole et al. 2000a), and intergalactic H I absorption (Baugh et al. 1998), and the isophotal selection effect in a very simple way (Cole et al. 2000a). However, as stressed by TY00, any predictions based on number count analyses will be seriously compromised unless all of the selection effects considered in this paper are taken into account simultaneously.

Based on a hierarchical clustering scenario in the CDM universe, the SAM naturally involves the merger-driven number evolution of galaxies, which has been introduced only phenomenologically in traditional models of galaxy evolution (Yoshii 1993; Yoshii & Peterson 1995; TY00). The fact that we have essentially reached the same conclusion from phenomenological approach confirms that previous simple prescriptions of the number evolution of galaxies are still useful in studying the global evolution of faint galaxies. It should be noted that in TY00 the adopted number evolution law which reproduces the observational data is $\phi_* \propto (1+z)$ and $L_* \propto (1+z)^{-1}$, and is consistent with the observational estimate of the merger rate of the Canada-France redshift survey (CFRS) galaxies (Le Févre et al. 2000).

The basic ingredients in the SAM analysis include the SF process and SN feedback. Although the constant and dynamical SFs can equally reproduce the local luminosity function by adjustment of their free parameters, we find that the dynamical SF predicts the formation of too many high-*z* galaxies to be consistent with the photometric redshift distribution of faint HST galaxies. Thus, our SAM analysis prefers the constant SF, as is also supported from other recent SAM analyses on the formation of quasars (Kauffmann & Haehnelt 2000) and the evolution of damped Ly-α systems (Somerville, Primack & Faber 2001).

The SN feedback, associated with the virial equilibrium for the baryonic component, controls the resulting size versus luminosity relation of elliptical galaxies. However, our SAM analysis is unable to reproduce the observed relation bifurcating into the giant-dwarf and giant-compact sequences; our brighter ellipticals reside on the bright portion of giant-dwarf sequence and our fainter ellipticals on the faint portion of giant-compact sequence. Although this limitation of our SAM analysis is found to hardly affect the conclusion in this paper, it is of urgent importance for the SAM to be equipped with some mechanism enabling the bifurcation of early-type galaxies into two distinct sequences as observed.

APPENDIX

A. BULGE SIZE AND SUPERNOVA FEEDBACK

In §4.2.2 we mentioned that the intrinsic size of early-type galaxies is related to the strength of SN feedback. In §2.1 describing SN re-heating the baryonic mass in a halo is given by $M_{\rm b} \lesssim \Omega_{\rm b} M_{\rm H}/(1+\beta)$, where $\beta \equiv \tau_*/\tau_{\rm reheat}$ and $M_{\rm H}$ is the halo mass. The left- and right-hand sides are not equal to each other, because this relation depends on the merging history of halos. The spherical collapse model gives $M_{\rm H} \propto V_{\rm circ}^3$, ignoring the dependence on the formation redshift. Thus, we obtain $r_{\rm e} \propto M_{\rm b}/V_{\rm circ}^2 \propto V_{\rm circ}/(1+\beta)$. Assuming a constant ratio of baryonic mass $M_{\rm b}$ relative to luminosity L, two limiting cases of $\beta \ll 1$ and $\beta \gg 1$ give

$$\log r_{\rm e} = \begin{cases} -\dfrac{1}{7.5}\mathcal{M} + \text{const.} & \text{for} \quad \beta \ll 1 \\ -\dfrac{(1+\alpha_{\rm hot})}{2.5(3+\alpha_{\rm hot})}\mathcal{M} + \text{const.} & \text{for} \quad \beta \gg 1, \end{cases} \tag{A1}$$

where $\mathcal{M}$ is the absolute magnitude. Fig. A13 shows the size of early-type galaxies for the SC model (*upper thick curve*) and the LC model (*lower thick curve*). The vertical scale is chosen arbitrarily to avoid overlapping. Solid lines are for $\beta \ll 1$ in equation

(A1). Dot-dashed and dashed lines are for $\beta \gg 1$ with $\alpha_{\rm hot}$ = 5.5 and 2.5, respectively (see Table A1). Although we fixed the baryon fraction, the baryonic mass-to-light ratio, and the formation redshift of halos, theoretical results (*thick curves*) can readily fit the scaling relations. This indicates that the SN feedback process essentially determines the size of early-type galaxies. In other words, we can constrain the SN feedback from reproducing their observed size versus luminosity relation. It should be noted that the importance of SN feedback in galaxy evolution has also been highlighted in other recent SAM analyses of the color versus magnitude relation of early-type galaxies (Kauffmann & Charlot 1998; Nagashima & Gouda 1999).

We would like to thank T. C. Beers for his critical reading of the manuscript. This work has been supported in part by the Grant-in-Aid for the Center-of-Excellence research (07CE2002) and for the Scientific Research Funds (10640229 and 12047233) of the Ministry of Education, Science, Sports and Culture of Japan.

REFERENCES

Arimoto, N., & Yoshii, Y. 1986, A&A, 164, 260
Arimoto, N., & Yoshii, Y. 1987, A&A, 173, 23
Arimoto, N., Yoshii, Y., & Takahara, F. 1991, A&A, 253, 21
Bardeen, J. M., Bond, J. R., Kaiser, N., & Szalay, A. S. 1986, ApJ, 304, 15
Baugh, C. M., Cole, S., & Frenk, C. S. 1996, MNRAS, 283, 1361
Baugh, C. M., Cole, S., Frenk, C. S., & Lacey, C. G. 1998, ApJ, 498, 504
Bender, R., Burstein, D., & Faber, S. M. 1992, ApJ, 399, 462
Binney, J., & Tremaine, S. 1987, Galactic Dynamics, Princeton Univ. Press, Princeton, NJ
Blanton, M.R. et al. 2000, preprint, astro-ph/0012085
Bond, J. R., Cole, S., Efstathiou, G., & Kaiser, N. 1991, ApJ, 379, 440
Bower, R. 1991, MNRAS, 248, 332
Cole, S., Aragon-Salamanca, A., Frenk, C. S., Navarro, J. F., & Zepf, S. E. 1994, MNRAS, 271, 781
Cole, S., Lacey, C. G., Baugh, C. M., & Frenk, C. S. 2000a, MNRAS, 319, 168
Cole, S. et al. 2000b, preprint, astro-ph/0012429
Eke, V. R., Cole, S., & Frenk, C. S. 1996, MNRAS, 282, 263
Fall, S. M. 1983, in 'Internal kinematics and dynamics of galaxies', proceedings of the IAU symposium 100, Besancon, France, Dordrecht, D. Reidel, p.391
Fernández-Soto, A., Lanzetta, K. M., & Yahil, A. 1999, ApJ, 513, 34
Folkes, S. et al. 1999, MNRAS, 308, 459
Furusawa, H., Shimasaku, K., Doi, M., & Okamura, S. 2000, ApJ, 534, 624
Gardner, J. P., Sharples, R. M., Carrasco, B. E., & Frenk, C. S. 1996, MNRAS, 282, L1
Gardner, J. P., Sharples, R. M., Frenk, C. S., & Carrasco, B. E. 1997, ApJ, 480, L99
Hall, P., & Mackay, C. B. 1984, MNRAS, 210, 979
Heyl, J. S., Cole, S., Frenk, C. S., & Navarro, J. F. 1995, MNRAS, 274, 755
Huchtmeier, W. K., & Richter, O. -G. 1988, A&A, 203, 237
Impey, C.D., Sprayberry, D., Irwin, M. J., & Bothun, G. D. 1996, ApJS, 105, 209
Jones, L.R., Fong, R., Shanks, T., Ellis, R. S., & Peterson, B. A. 1991, MNRAS, 249, 481
Kauffmann, G., & Charlot, S. 1998, MNRAS, 294, 705
Kauffmann, G., & Haehnelt, M. 2000, MNRAS, 311, 576
Kauffmann, G., White, S. D. M., & Guiderdoni, B. 1993, MNRAS, 264, 201
Kodama, T., & Arimoto, N. 1997, A&A, 320, 41
Koo, D.C. 1986, ApJ, 311, 651
Lacey, C.G., & Cole, S. 1993, MNRAS, 262, 627
Le Févre, O., et al. 2000, MNRAS, 311, 565
Loveday, J., Peterson, B. A., Efstathiou, G., & Maddox, S. J. 1992, ApJ, 90, 338
Maddox, S. J., Sutherland, W. J., Efstathiou, G., Loveday, J., & Peterson, B. A. 1990, MNRAS, 247, 1p
Makino, J., & Hut, P. 1997, ApJ, 481, 83
Metcalfe, N., Shanks, T., Fong, R., & Jones, L. R. 1991, MNRAS, 249, 498
Mobasher, B., Sharples, R. M., & Ellis, R. S. 1993, MNRAS, 263, 560
Nagashima, M., & Gouda, N. 1999, preprint, astro-ph/9906184
Peebles, P. J. E. 1993, Principles of Physical Cosmology, Princeton Univ. Press, Princeton, NJ
Press, W., & Schechter, P. 1974, ApJ, 187, 425
Ratcliffe, A., Shanks, T., Parker, Q., & Fong, R. 1998, MNRAS, 293, 197
Simien, F., & de Vaucouleurs, G. 1986, ApJ, 302, 564
Somerville, R.S., & Kolatt, T. 1999, MNRAS, 305, 1
Somerville, R.S., & Primack, J. R. 1999, MNRAS, 310, 1087
Somerville, R.S., Primack, J. R., & Faber, S. M. 2001, MNRAS, 320, 504
Sutherland, R., & Dopita, M. A. 1993, ApJS, 88, 253
Suzuki, T.K., Yoshii, Y., & Beers, T.C. 2000, ApJ, 540, 99
Totani, T., & Yoshii, Y. 2000, ApJ, 540, 81 (TY00)
Tyson, J.A. 1988, AJ, 96, 1
Wang, B., & Heckman, T. 1996, ApJ, 457, 645
Williams, R. T. et al. 1996, AJ, 112, 1335
Yoshii, Y. 1993, ApJ, 403, 552
Yoshii, Y., & Peterson, B. A. 1991, ApJ, 372, 8
Yoshii, Y., & Peterson, B. A. 1994, ApJ, 436, 551
Yoshii, Y., & Peterson, B. A. 1995, ApJ, 444, 15
Yoshii, Y., & Takahara, F. 1988, ApJ, 326, 1
Zucca, E. et al. 1997, A&A, 326, 477

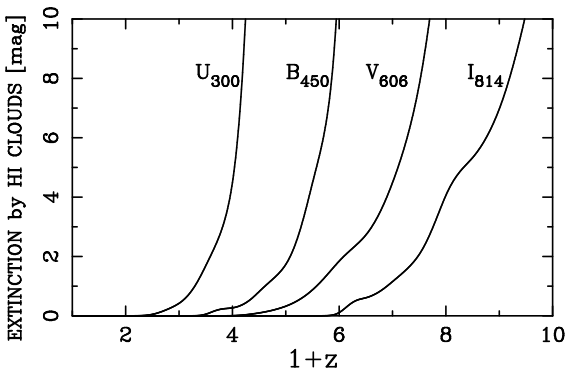

FIG. A1.— Extinction in units of magnitude by intervening intergalactic H I clouds for four HDF passband filters. The model optical depth is taken from Yoshii & Peterson (1994).

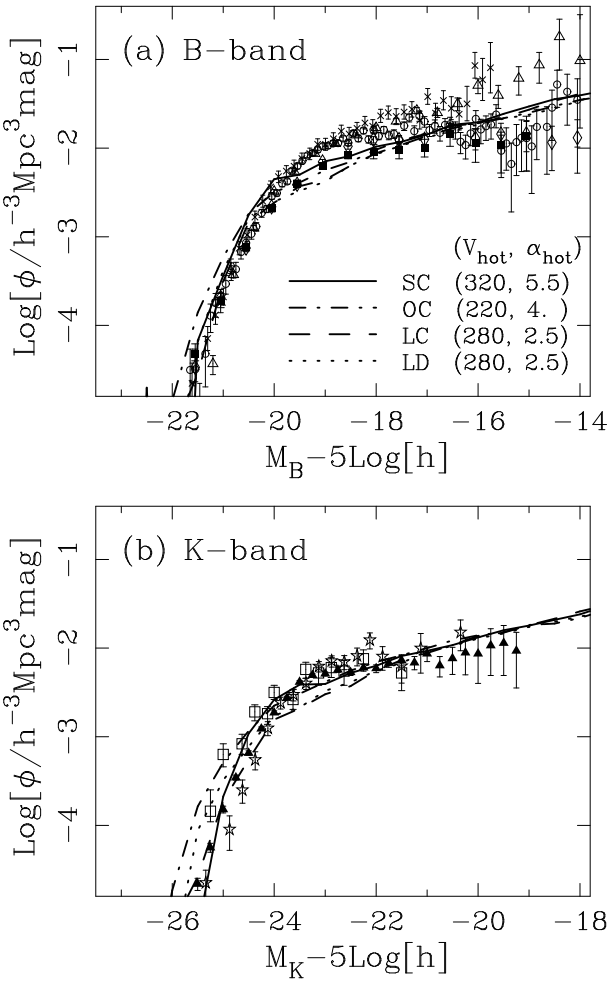

FIG. A2.— Local luminosity functions in the (a) *B* band and (b) *K* band. The solid, dot-dashed, dashed, and dotted lines indicate the SC, OC, LC and LD models, respectively. Symbols with errorbars in (a) indicate the observational data from APM (Loveday et al. 1992, *filled squares*), ESP (Zucca et al. 1997, *open triangles*), Durham/UKST (Ratcliffe et al. 1998, *open diamonds*), 2dF (Folkes et al. 1999, *open circles*), and SDSS (Blanton et al. 2000, *crosses*). Note that the SDSS luminosity function shown here is that with the same detection limit as employed in the 2dF survey. Symbols in (b) indicate the data from Mobasher et al. (1993, *open squares*), Gardner et al. (1997, *open stars*), and 2MASS (Cole et al. 2000b, *filled triangles*).

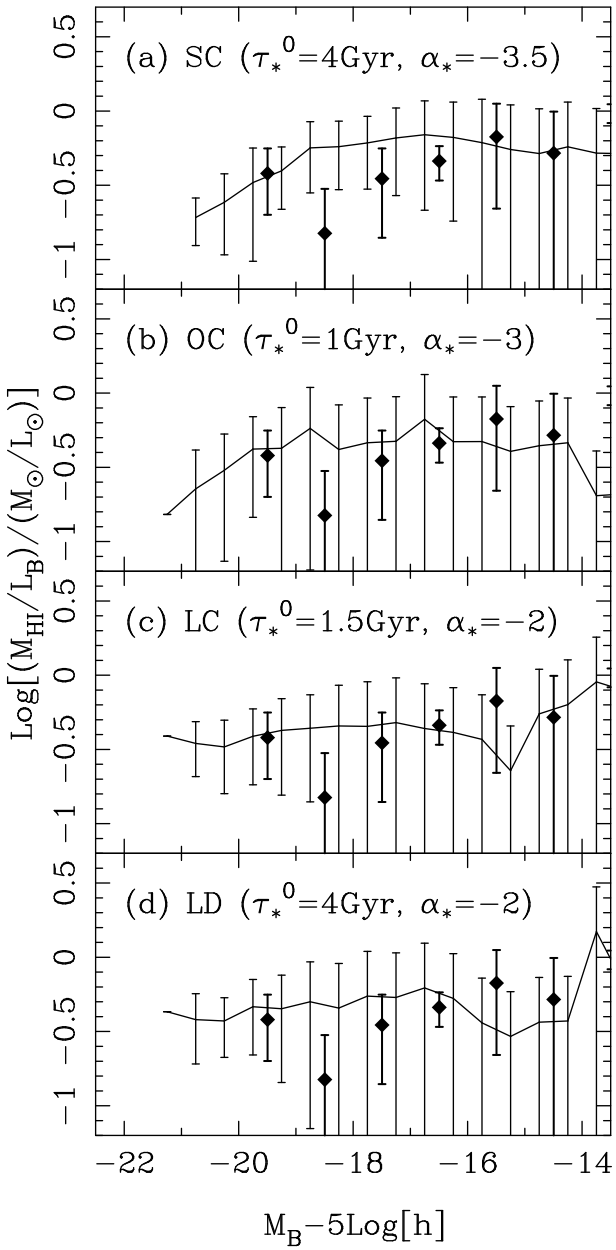

FIG. A3.— Cold gas mass relative to *B*-band luminosity of spiral galaxies. Solid curves in the four panels from top to bottom show the SC, OC, LC and LD models, respectively. Errorbars denote 1σ scatters. Filled diamonds indicate the observational data for atomic neutral hydrogen taken from Huchtmeier & Richter (1988). In the models, the cold gas consists of all species of elements, therefore its mass is multiplied by 0.75, i.e., $M_{\rm HI} = 0.75 M_{\rm cold}$, which corresponds to the fraction of hydrogen. Because the observational data denote only atomic hydrogen, they should be interpreted as lower limits of the ratio.

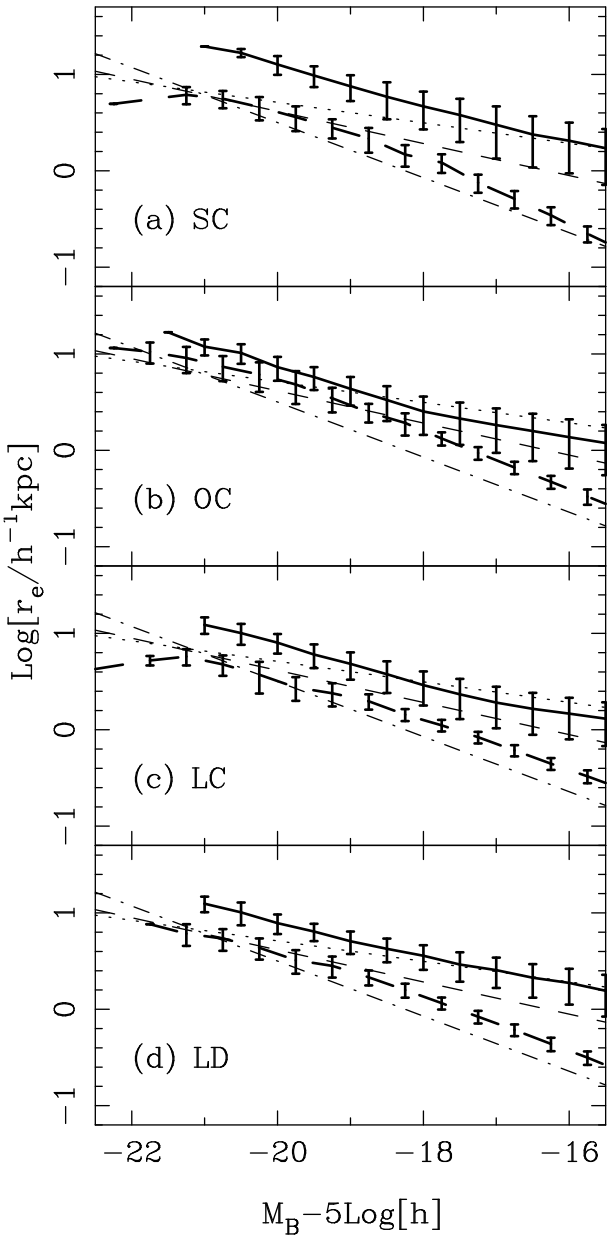

FIG. A4.— Galaxy sizes. The thick solid lines and the thick dashed lines show theoretical results for effective radii of late-type and early-type galaxies, respectively. Errorbars denote 1σ scatters. The thin dotted lines, the thin dashed lines, and the thin dot-dashed lines show the observed best-fit relations given by TY00 for spirals, dwarf ellipticals and compact ellipticals, respectively. The original data are given by Impey et al. (1996) for spirals and Bender et al. (1992) for ellipticals.

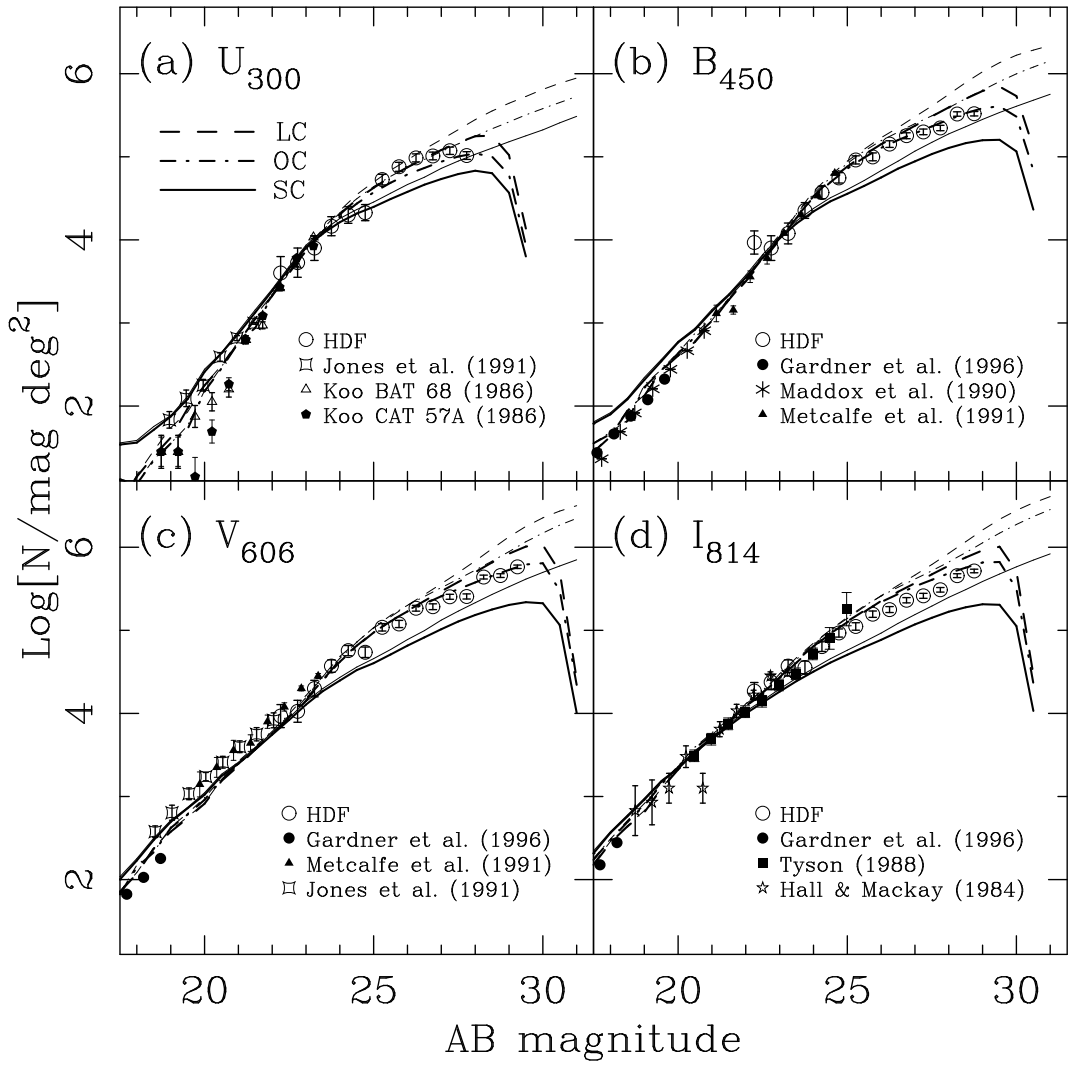

FIG. A5.— Number-magnitude relations for various cosmological models. The solid, dot-dashed, and dashed lines indicate SC, OC, and LC, respectively. The thick lines denote models including the selection effects and the absorption effect by intergalactic H I clouds, while the thin lines denote those without the effects. The symbols indicate observational data.

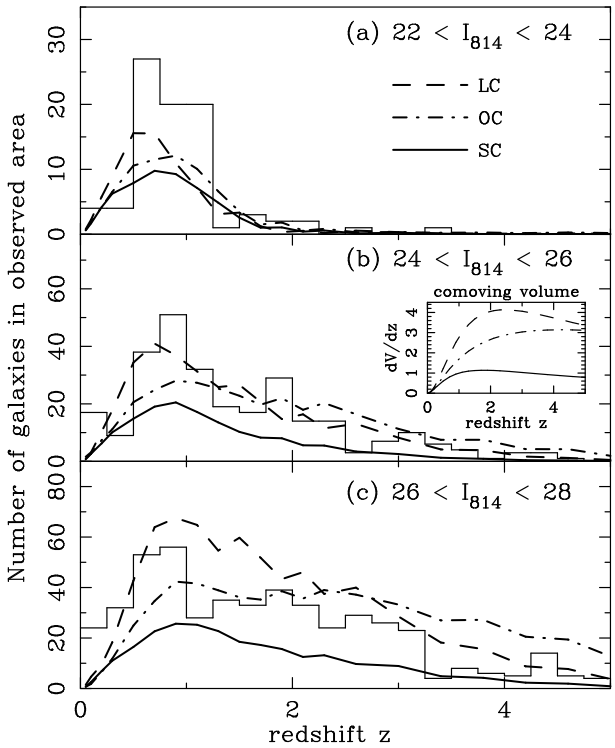

FIG. A6.— Redshift distributions for various cosmological models. The types of lines are the same as Fig. A5, but for only models including the effects of the selection and the absorption by the H I clouds. The histograms indicate the photometric redshift distribution of the HDF. For reference, the redshift dependence of the comoving volume element dV/dz in units of $10^6 h^{-3}\mathrm{Mpc}^3$ is shown in the middle panel for the three cosmological models. The types of lines are the same as corresponding cosmological models for the redshift distributions of galaxies.

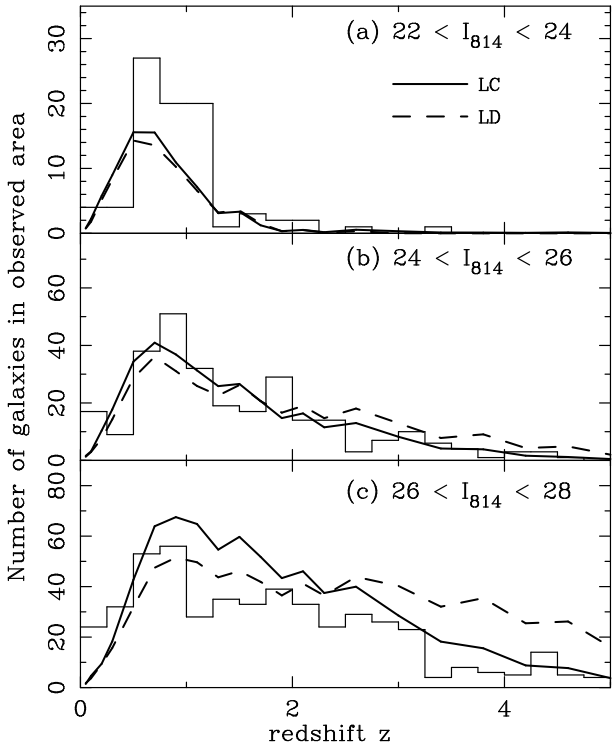

FIG. A8.— Redshift distributions. The solid lines and the dashed lines indicate the LC and LD models, respectively. The histograms indicate the photometric redshift distribution of the HDF.

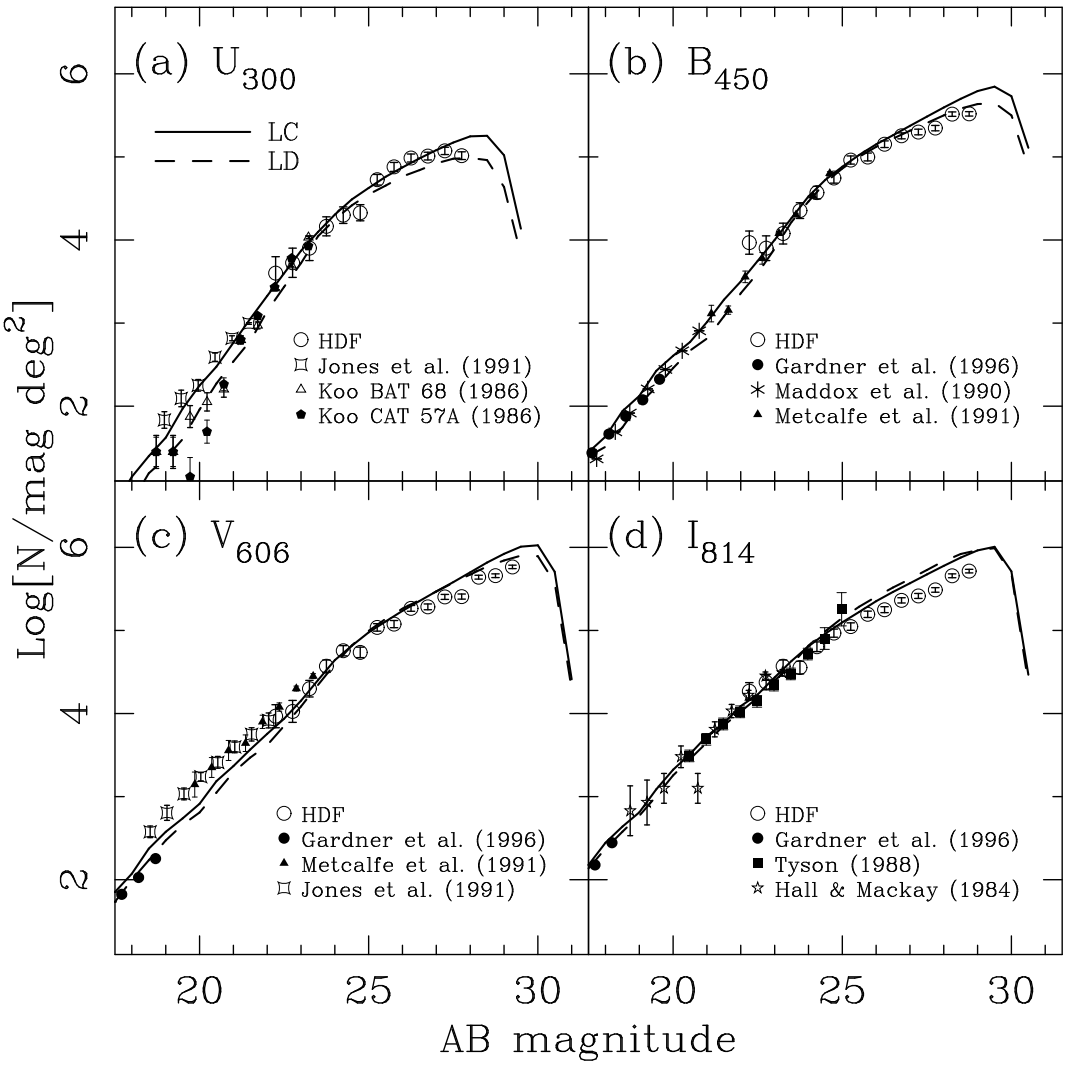

FIG. A7.— Number-magnitude relations. The solid lines and the dashed lines indicate the LC (CSF) and LD (DSF) models, respectively.

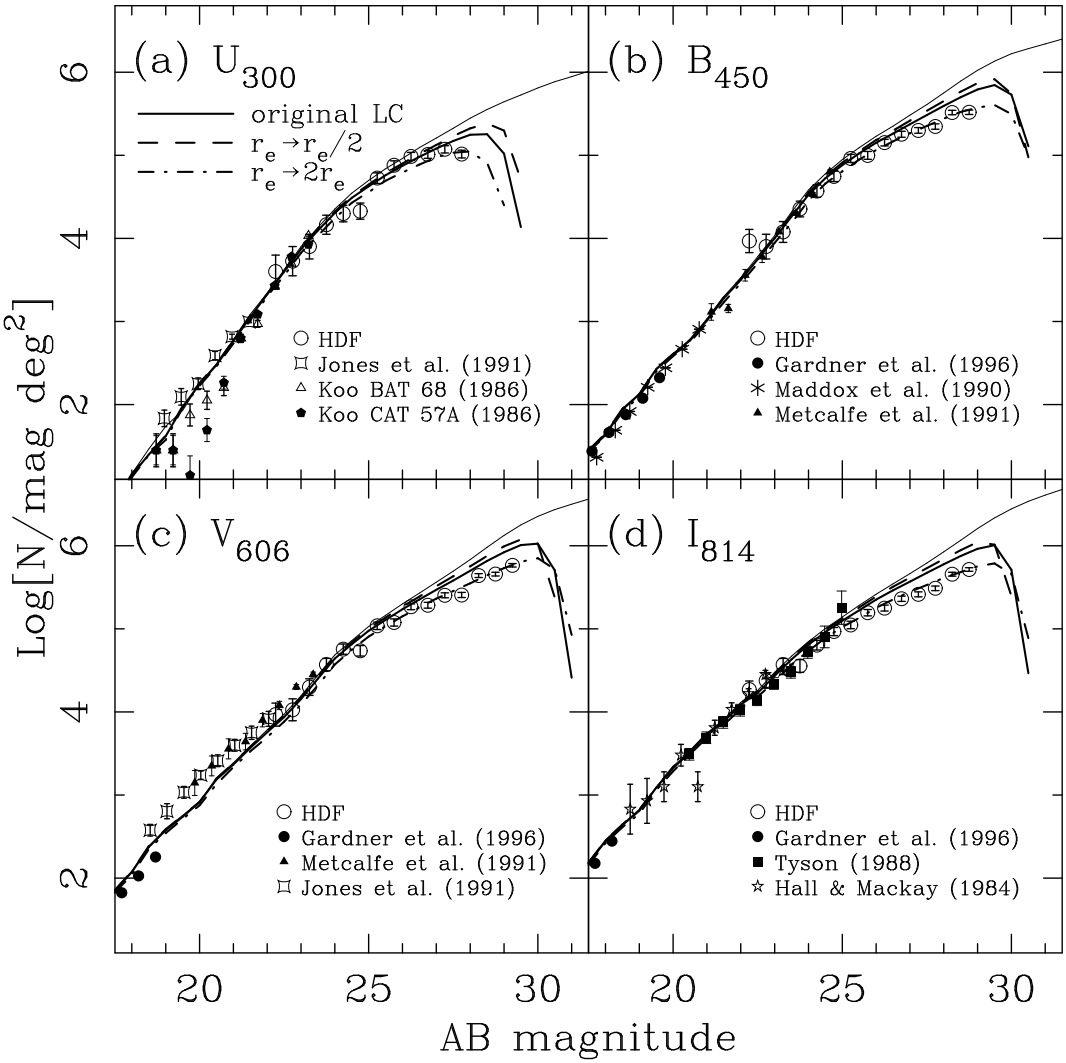

FIG. A9.— Number-magnitude relations. The solid lines indicate the original LC model. The thick and thin lines denote models with and without the selection effects. The dashed lines and the dot-dashed lines indicate the high and low surface brightness models, respectively.

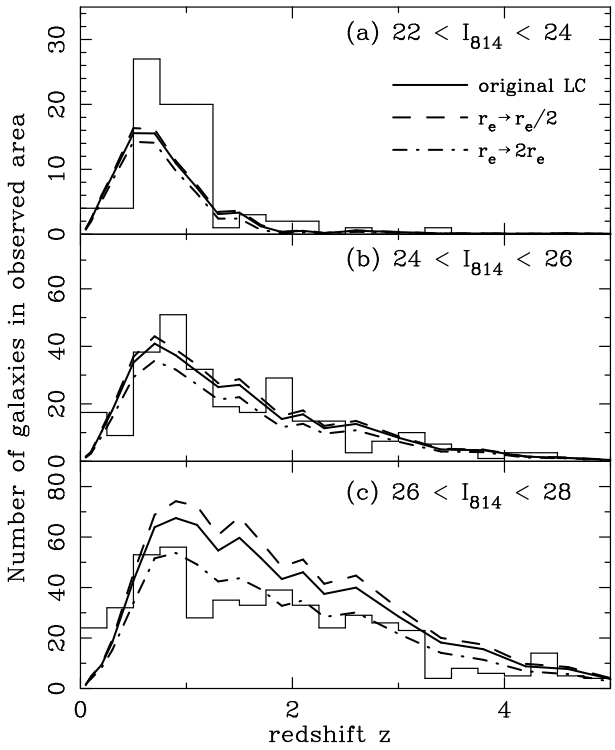

FIG. A10.— Redshift distributions. The thick solid lines indicate the LC model. The dashed and dot-dashed lines denote the high and low surface brightness models for the model LC, respectively. The histograms indicate the photometric redshift distribution of the HDF.

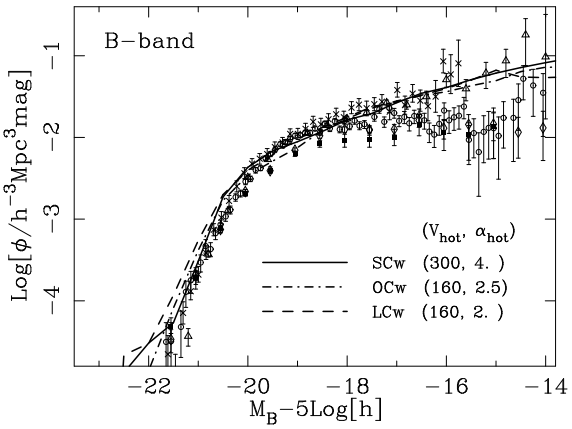

FIG. A11.— Local luminosity function in the *B*-band. The solid, dot-dashed and dashed lines indicate the SCw, OCw and LCw models, respectively. The types of symbols denote observations and are the same as Fig. A2a.

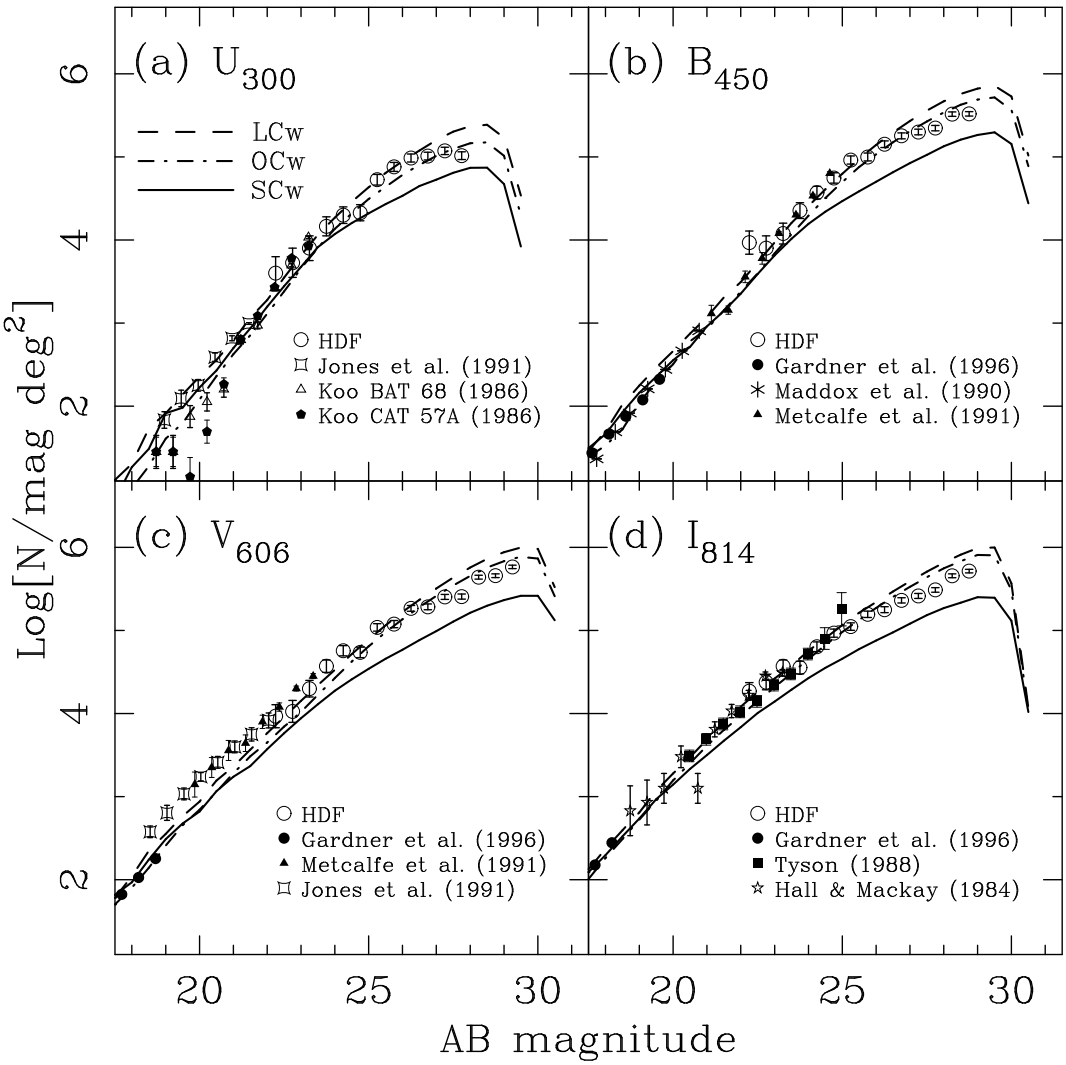

FIG. A12.— Number-magnitude relations. The same as Fig. A5 but for the model SCw, OCw and LCw. The types of lines are the same as Fig. A11.

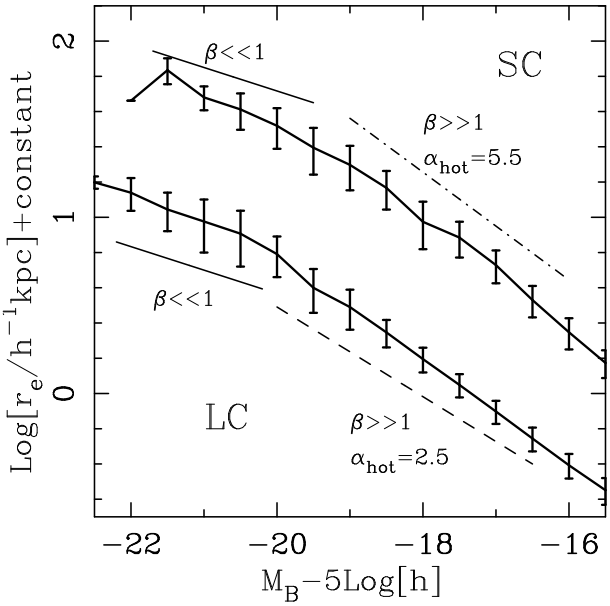

FIG. A13.— Galaxy sizes in arbitrary unit. The upper and lower thick lines indicate effective radius of early-type galaxies in the SC and LC models, respectively. The thin solid lines indicate the case of $\beta \ll 1$ and the thin dot-dashed line and the thin dashed line indicate the case of $\beta \gg 1$ with $\alpha_{\rm hot}$ = 5.5 and 2.5, respectively.

TABLE A1

MODEL PARAMETERS

	cosmological parameters				astrophysical parameters						
CDM Model	Ω_0	Ω_Λ	h	σ_8	$V_{\rm hot}$ (km s^{-1})	$\alpha_{\rm hot}$	τ_*^0 (Gyr)	α_*	$f_{\rm bulge}$	$f_{\rm b}$	Υ
SC	1	0	0.5	0.67	320	5.5	4	-3.5	0.2	1	1.
OC	0.3	0	0.6	1	220	4	1	-3	0.5	0.5	1.5
LC	0.3	0.7	0.7	1	280	2.5	1.5	-2	0.5	0.5	1.5
LD	0.3	0.7	0.7	1	280	2.5	4	-2	0.5	0.5	1.5

TABLE A2

PARAMETERS FOR WEAK FEEDBACK MODELS

	cosmological parameters				astrophysical parameters						
CDM Model	Ω_0	Ω_Λ	h	σ_8	$V_{\rm hot}$ (km s^{-1})	$\alpha_{\rm hot}$	τ_*^0 (Gyr)	α_*	$f_{\rm bulge}$	$f_{\rm b}$	Υ
SCw	1	0	0.5	0.67	300	4	4	-2.5	0.2	1	1
OCw	0.3	0	0.6	1	160	2.5	1.5	-1.5	0.5	0.5	1.8
LCw	0.3	0.7	0.7	1	160	2	1.5	-1.5	0.5	0.5	1.5